Case Studies in Construction Materials 22 (2025) e04503

Contents lists available at ScienceDirect

Case Studies in Construction Materials

journal homepage: www.elsevier.com/locate/cscm

Case study

Comparative study on dynamic compressive properties and sustainability assessment of one-part fiber-reinforced geopolymer composites

Hanyuan Shi [a,b], Qian Zang [c], Yingfan Wang [b], Haimin Qian [a,*], Zhouhong Zong [c], Jingming Cai [b,d], Mei Li [e], Yuanzheng Lin [a,c,**]

[a] *Zhejiang Engineering Research Center of Intelligent Urban Infrastructure, Hangzhou City University, Hangzhou 310015, China*
[b] *School of Civil Engineering, Southeast University, Nanjing, Jiangsu 211189, China*
[c] *Engineering Research Center of Safety and Protection of Explosion & Impact of Ministry of Education (ERCSPEIME), Southeast University, Nanjing, Jiangsu 211189, China*
[d] *Faculty of Civil and Environmental Engineering, TU Darmstadt, Franziska-Braun-Straße, Darmstadt, Germany*
[e] *School of Civil Engineering, Suzhou University of Science and Technology, 1701 Binhe Road, Suzhou, Jiangsu 215011, China*

ARTICLE INFO

Keywords:
One-part fiber-reinforced geopolymer composites (OP-FRGC)
Split Hopkinson pressure bar
Dynamic compressive properties
Sustainability
Cost

ABSTRACT

Although geopolymers can significantly reduce carbon dioxide emissions, their widespread application is limited due to the requirement for alkaline activation solutions. The recently developed "one-part geopolymer" overcomes this limitation by using a solid alkaline activator, thereby enhancing construction convenience while maintaining performance comparable to conventional alkaline solution activated geopolymers or cement-based materials. In this study, a split Hopkinson pressure bar (SHPB) was employed to investigate the dynamic properties of one-part fiber-reinforced geopolymer concrete (OP-FRGC), focusing on different types of fibers. The compressive dynamic increase factor (CDIF), energy absorption capacity, and failure modes of OP-FRGC under dynamic loading were analyzed. The results indicate that the incorporation of fibers changes the failure mode of OP-FRGC from brittle to ductile, significantly enhancing its toughness. OP-FRGC exhibited strain rate sensitivity, with the CDIF showing an approximate logarithmic increase with the strain rate. In addition, a comprehensive evaluation of OP-FRGC incorporating different fiber types was conducted, considering mechanical properties, sustainability, and cost. This study offers a useful reference for understanding the dynamic behavior of OP-FRGC, thereby promoting its potential in practical engineering applications.

1. Introduction

The fields of civil buildings, industrial plants, road traffic, and related sectors heavily rely on ordinary Portland cement (OPC). However, OPC is primarily responsible for carbon dioxide emissions, which play a major role in global warming. To address the conflict between the growing global demand for construction materials and environmental sustainability, geopolymer concrete (GC)

* Corresponding author.
** Corresponding author at: Zhejiang Engineering Research Center of Intelligent Urban Infrastructure, Hangzhou City University, Hangzhou 310015, China.
E-mail addresses: qianhm@hzcu.edu.cn (H. Qian), 103200086@seu.edu.cn (Y. Lin).

https://doi.org/10.1016/j.cscm.2025.e04503
Received 15 November 2024; Received in revised form 17 February 2025; Accepted 5 March 2025
Available online 6 March 2025

has been proposed and extensively studied [1–4]. Research indicates that compared to OPC, geopolymers made from industrial by-products can reduce carbon emissions by about 70 % [5].

While GC offers less carbon emissions than conventional cement-based concrete, its practical application remains limited. The need for a high concentration of alkaline activator solution in GC production poses risks such as skin burns and respiratory issues, limiting its widespread application. Recently, the "one-part geopolymer" (OPG), also referred to as "just-add-water geopolymer", has emerged as a promising solution for practical engineering applications [6–9]. One-part geopolymer concrete (OP-GC) uses solid alkaline activator, which reduces handling risks, such as chemical burns, and enhances the safety of the construction process. This advancement not only enhances practicality but also maintains mechanical performance comparable to traditional cement-based materials, expanding the potential of GC for practical engineering applications [10,11].

Fibers have been successfully incorporated into geopolymer concrete to enhance its toughness [12]. Recently, different types of fibers have been added in an effort to develop fiber-reinforced geopolymer composite (FRGC) with enhanced performance. FRGC demonstrates significantly higher ductility compared to conventional GC, utilizing the fiber bridging effect, where fibers hold the cracked matrix together and control crack propagation under loading. Notably, FRGC exhibits strain-hardening behavior under tension, substantially enhancing the energy absorption capacity of GC—an improvement particularly valuable in protective engineering applications [13]. Numerous research efforts have focused on investigating the dynamic behavior of GC and FRGC under blast and impact loads [14–16], often employing split Hopkinson pressure bar (SHPB) to reveal their dynamic properties [17]. For instance, Xin et al. [18] utilized SHPB to investigate the strength, deformation, and energy absorption of GC under dynamic loading, finding that energy absorption and strength increased significantly with the strain rate. According to Xiao et al. [19], while polyvinyl alcohol (PVA) fibers improved the impact performance of GC, increasing fly ash content had a detrimental effect. Khan et al. [20,21] studied the dynamic mechanical behavior of FRGC with steel and polyethylene (PE) fibers under both compressive and splitting tensile conditions, concluding that the addition of fibers significantly enhanced the toughness and energy absorption capacity of GC. Zhong et al. [22] found that engineered geopolymer composite (EGC) incorporating a combination of PVA and recycled type polymer (RTP) fibers demonstrated improved dynamic compressive strength, energy absorption capacity, enhanced toughness, and reduced post-test damage compared to traditional EGC with PVA fibers alone. The research demonstrates that incorporating RTP fibers effectively mitigates the reduction in flowability and quasi-static compressive strength caused by PVA fibers. Similarly, the impacts of steel, polypropylene (PP), and hybrid steel-PP fibers on the dynamic compressive characteristics of FRGC were examined by Zhang et al. [23], reporting that specimens with PP fibers exhibited more sensitivity to strain rate than steel fibers. Xu et al. [24] and Lao et al. [25–27] employed PE fibers to develop EGC, which exhibit high compressive strength and remarkable ductility. The mechanical properties and microstructural characteristics of these EGC were also examined from various perspectives, including alkali content, water-cement ratio, and raw material type. All these studies have highlighted the strain rate dependency of FRGC and the effectiveness of fiber reinforcement in improving toughness. However, all these investigations utilized conventional geopolymer composites activated by alkaline solutions, which inherently involve safety hazards and complexities in preparation. It is noteworthy that the authors recently reported the dynamic characteristics of one-part high performance geopolymer composites, demonstrating its potential for use in protective engineering [28,29]. This recent development signifies the promising prospects of one-part geopolymer composites in addressing the challenges associated with traditional geopolymer systems while providing effective solutions for demanding engineering applications.

It has been noted that OP-GC generally exhibits properties comparable to conventional GC [30–32], however, differences between their respective fiber-reinforced composites, i.e., one-part FRGC (OP-FRGC) and alkaline solution activated FRGC [33], are still not fully understood. In particular, the dynamic behavior of OP-FRGC has yet to be thoroughly investigated. Furthermore, previous studies have used varying geopolymer matrix designs, leading to weak comparability across different fiber types. Given the scarcity of research and the significant potential of OP-FRGC in protective engineering, it is crucial to examine its dynamic properties, such as failure mode, energy absorption capacity, and compressive dynamic increase factor (CDIF), which are vital for ensuring resilience against impacts and blasts.

The objective of this research is to examine the dynamic compressive behavior of OP-FRGC, with a particular emphasis on the impact of various fiber types on CDIF, energy absorption, and failure mode. To facilitate a comprehensive comparison, OP-GC specimens were also tested. In addition, CDIFs of OP-FRGC were compared to those of traditional GC and FRGC reported in existing literature. Finally, the comprehensive performance of OP-FRGC was evaluated, considering mechanical properties, sustainability, and cost.

2. Material design and experimental program

2.1. Material design

The OPG involved in the present study was a recently developed binder material [34–36] that generally behaves similarly to OPC.

Table 1
Chemical compositions of raw materials (wt%).

Type	SiO_2	Al_2O_3	CaO	Fe_2O_3	MgO	K_2O	Na_2O	SO_3
FA	50.23	28.84	5.36	6.54	1.89	2.76	1.83	1.01
GGBS	34.49	15.56	34.78	1.27	7.28	1.94	1.72	1.34

The main constituents of OPG were precursors and activators. Fly ash (FA) and ground granulated blast-furnace slag (GGBS) functioned as precursors, while sodium silicate powder and sodium metasilicate powder were activators, which made up 10 % of the precursors by weight. The primary chemical compositions of GGBS and FA are listed in Table 1. The water-binder ratio was set as 0.24, and the sand-binder ratio was set as 0.6. Moreover, high-range water reducer (HRWR) was employed with a weight dosage of 0.5 % to achieve better workability and benefit the dispersibility of chopped fibers [37]. The technical parameters of HRWR are detailed in Table 2. The raw materials and their particle size distribution are shown in Fig. 1.

In order to investigate the impact of fiber type on the dynamic mechanical properties of OP-FRGC, a volume content of 1 % was added to OP-GC separately with three different types of polymer fibers: PVA, PE, and PP. For clear demonstration, the composites reinforced by different types of fibers were denoted by OP-FRGC-PVA, OP-FRGC-PE, and OP-FRGC-PP, respectively. Table 3 shows the properties of these polymer fibers. In particular, these three types of fibers shared a close length and density. Among the three types of fibers, PE fiber had the strongest elastic modulus and tensile strength, while PP fiber had the lowest. In addition, PE fiber had the highest cost and PP fiber exhibited the lowest cost. For comparison, OP-GC specimens without fiber were also prepared as a reference. Table 4 lists the material mix design for all the material types in the present study.

The preparation process of OP-FRGC is depicted in Fig. 2. First, a homogeneous solid mixture was prepared by blending one-part geopolymer with quartz sand for one minute. Water was then incorporated, followed by an additional two minutes of mixing to form the geopolymer mortar. Subsequently, 1.0 % volume fraction fibers were added to produce a uniform OP-FRGC paste, and the mixture was stirred for another 10 min. The OP-FRGC and OP-GC paste were poured into 50 mm × 50 mm × 50 mm molds and vibrated for 10 s. After one day, the molds were removed, and the specimens were kept in a curing environment with 95 % ± 3 % humidity and a temperature of 20 ± 2 °C for 28 days.

2.2. Experimental program

Fig. 3 shows the schematic of the SHPB system, which includes a data acquisition system, compressed gas cabin, striker bar, incident bar, transmission bar, and absorbing bar. The striker, incident, and transmission bars are made of steel alloy 60Si2Mn, with an elastic wave velocity of approximately 5100 m/s. The cylindrical striker has a diameter of 40 mm and a length of 0.5 m, while the incident and transmission bars have a square cross-sectional of 50 mm × 50 mm, with lengths of 2.5 m and 2.0 m, respectively. To reduce friction, grease was applied between the specimen and the adjacent bars before testing. In addition, a rubber pulse shaper was attached to the impact surface of the incident bar to minimize high-frequency wave oscillations. The striker bar was propelled at different speeds by varying pressure levels, producing different strain rates in the specimens. The data acquisition system recorded strain data to capture the incident, reflected, and transmitted waves during the experiment.

It should be noted that while cylindrical specimens are commonly used in most SHPB tests, this study employed cubic specimens with a side length of 50 mm to maintain consistency with the cross-sectional dimensions of the SHPB bars, which may introduce complex wave interactions due to dispersion and reflection [38]. However, this does not affect the comparative analysis among specimens with different fiber types, and the results are still considered valid for evaluating the dynamic compressive properties of OP-FRGC.

According to the one-dimensional stress wave propagation theory, the stress (σ), strain (ε), and strain rate ($\dot{\varepsilon}$) can be computed using the reflected strain (ε_r), transmission strain (ε_t), and the size and parameters of the bars and specimen [39]. The following are the formulas:

$$\sigma = \frac{E_b A_b}{A_0}\varepsilon_t \tag{1}$$

$$\dot{\varepsilon} = -\frac{2C_b}{L_0}\varepsilon_r \tag{2}$$

$$\varepsilon = -\frac{2C_b}{L_0}\int_0^t \varepsilon_r dt \tag{3}$$

where E_b, A_b and C_b symbolize the elastic modulus, cross-sectional area, and stress wave velocity of the bars, respectively; A_0 and L_0 represent the initial cross-sectional area and length of the specimen.

It is important to note that the above formula is valid only when the transmission wave is coincident with the sum of the incident and reflected waves [39]. A typical stress equilibrium state for all sample types during the experiments is depicted in Fig. 4. To ensure the validation of the data in the current study, the stress equilibrium was verified for every impact. According to previous research [40–42], the strain rate in this investigation was determined at the point at which the stress attained its maximum value.

In addition to the dynamic tests, quasi-static tests were carried out to provide a benchmark for dynamic mechanical characteristics.

Table 2
Parameters of HRWR.

Cost (CNY/t)	Water content (%)	Density (g/cm^3)	PH	Chloride content (%)	Sodium chloride content (%)
60000	1.81	0.6 ± 0.1	7.1	≤ 0.1	≤ 2.0

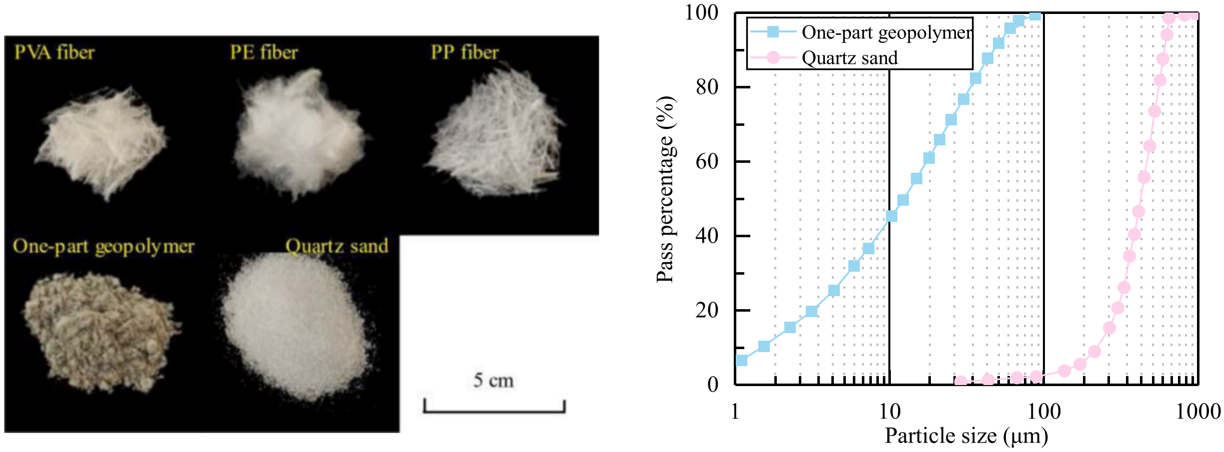

(a) Macroscopic morphology (b) Particle size distribution

Fig. 1. Raw materials.

Table 3
Characteristics of different polymer fibers.

Type	Cost (CNY/t)	Length (mm)	Diameter (μm)	Tensile strength (MPa)	Elastic modulus (GPa)	Density (g/cm^3)
PVA	60000	12	26	1560	36.3	1.3
PE	200000	12	24	2400	100	0.97
PP	44415	12	140	1000	12	0.91

Table 4
Mix design of the materials. (kg/m^3).

Material type	OPG				Quartz sand	Water	Fiber	HRWR
	FA	GGBS	Sodium silicate	Sodium metasilicate				
OP-GC	492.73	492.73	49.27	49.27	650.41	260.16	0	5.42
OP-FRGC-PP							9.08	
OP-FRGC-PE							9.68	
OP-FRGC-PVA							12.97	

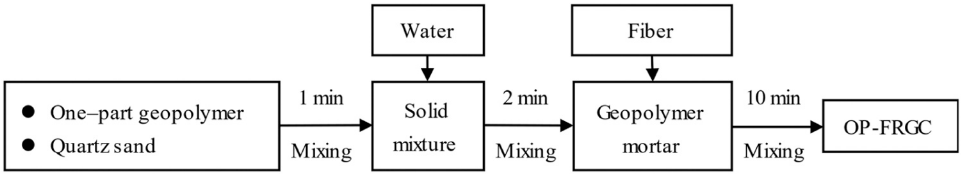

Fig. 2. Preparation process of OP-FRGC.

The test equipment is a 2000 kN universal hydraulic testing apparatus and the load rate was 0.3 mm/min.

3. Test results

3.1. Quasi-static test

Fig. 5 presents the quasi-static test results after 28 days of curing. As shown, the quasi-static compressive strength of OP-FRGC was lower than that of OP-GC. In particular, the compressive strength of OP-FRGC-PP was 34.1 MPa, which was about 65 % of that of OP-GC. In comparison, OP-FRGC-PVA exhibited a compressive strength of 45.1 MPa, while OP-FRGC-PE demonstrated a compressive strength close to that of OP-GC, reaching 51.3 MPa.

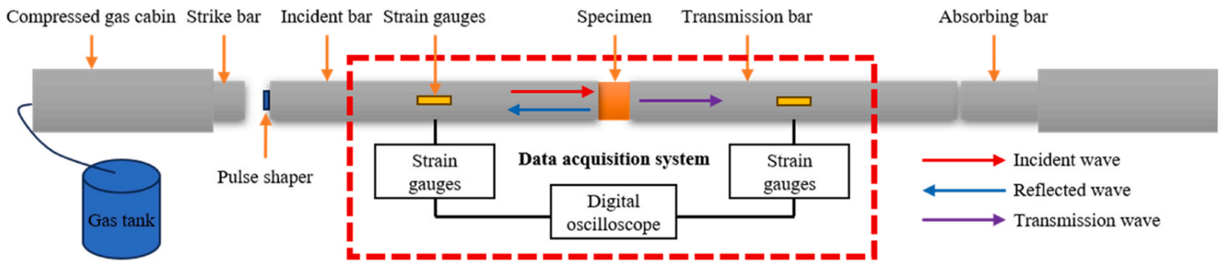

Fig. 3. SHPB system.

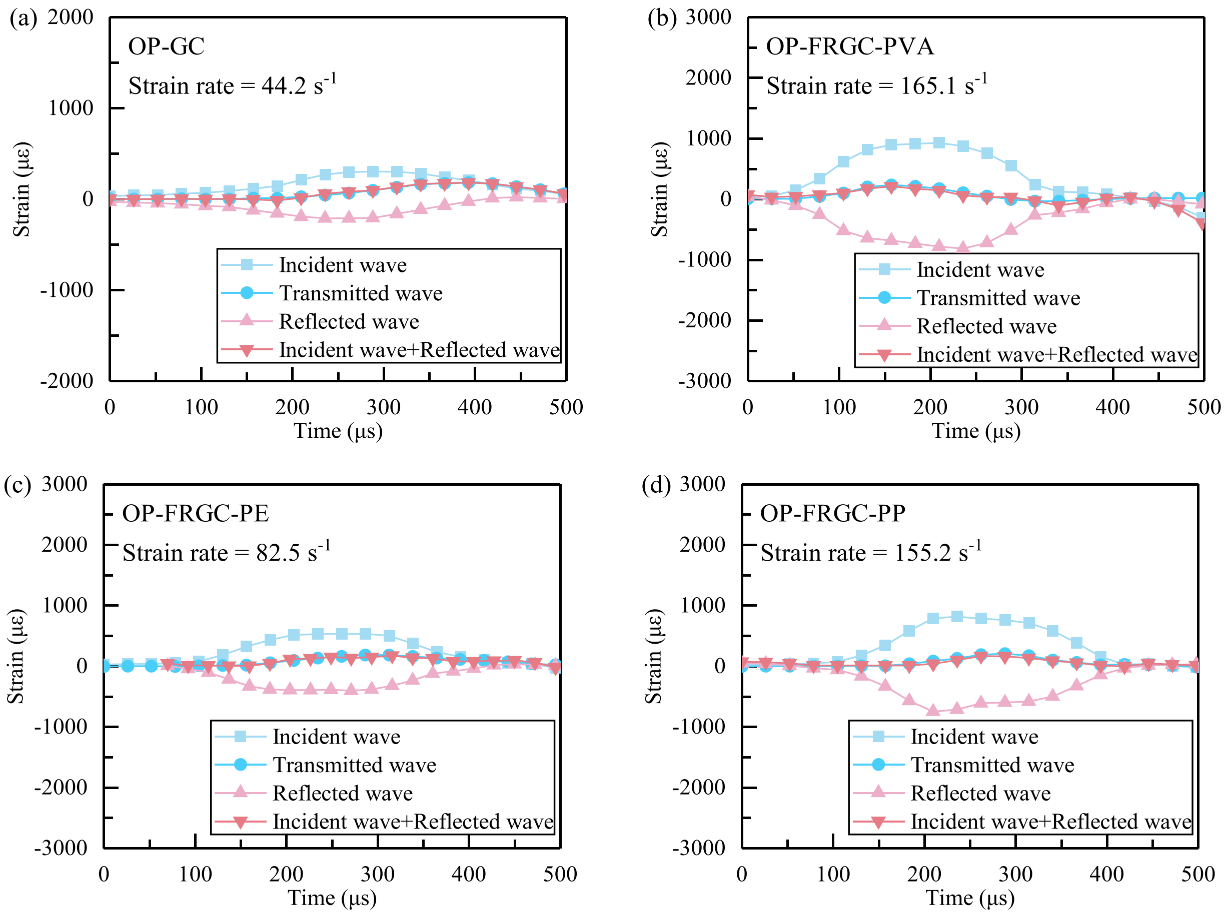

Fig. 4. A typical state of stress equilibrium.

The reduced compressive strength of OP-FRGC compared to OP-GC can be attributed to two primary factors. First, the addition of fibers occupies a certain volume within the matrix, thereby reducing the effective volume available to resist compression and preventing the mortar from achieving the expected strength [39,43]. Second, despite the use of water reducer, some fibers tended to clump together, making it difficult to achieve uniform dispersion, which subsequently caused internal defects. Similar to previous studies [19,20,22], the inclusion of fibers did not enhance the quasi-static compressive strength of the composites. Instead, it reduced strength due to potential matrix disturbance and increased porosity. However, this effect varies depending on the fiber type. In particular, PVA fibers were highly hydrophilic and prone to clumping, whereas PE fibers dispersed more readily, reducing void formation and limiting significant fiber agglomeration. As a result, OP-FRGC-PE maintained nearly the same strength as OP-GC, while OP-FRGC-PVA exhibited a 12.4 % reduction in strength compared to OP-GC. It is also noteworthy that the PP fibers, which had lower tensile strength and modulus of elasticity compared to PE and PVA fibers, led to the most pronounced reduction in compressive strength under quasi-static loading among the three fiber-reinforced composites.

Fig. 6 illustrates the failure modes of OP-GC and OP-FRGC under quasi-static loading. It can be seen that OP-GC exhibited brittle

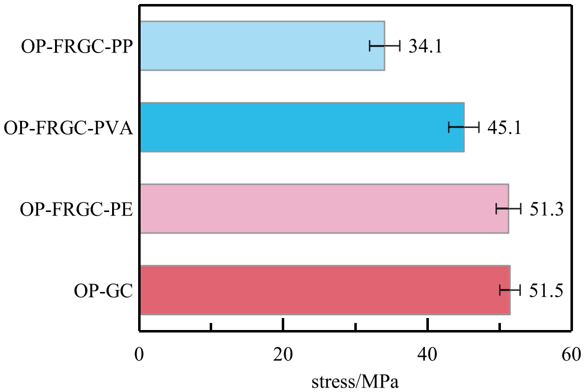

Fig. 5. Compressive strength of OP-FRGC and OP-GC under quasi-static load.

failure characterized by the formation of large fragments. In contrast, the failure mode of OP-FRGC differed significantly due to the incorporation of fibers, which altered the damage process and resulted in a more ductile failure mechanism. The OP-FRGC specimens displayed vertical cracking and radial expansion during compression, indicating improved energy dissipation. After loading, the fibers within OP-FRGC were observed to undergo significant deformation and, in some cases, were pulled out from the matrix. This behavior highlights the bridging effect of the fibers, which helped to slow down crack propagation and prevent failure by maintaining some integrity of the matrix even after extensive cracking.

3.2. Dynamic test

3.2.1. Failure mode

Fig. 7 shows the failure modes of OP-GC and OP-FRGC under dynamic compressive loading. It was observed that more severe damage occurred to the specimens as the strain rate increased. For each type of specimen, the cracks widened, and the resulting fragments became finer. When the strain rate reached 44.2 s^{-1} for OP-GC, 164.1 s^{-1} for OP-FRGC-PVA, 215.4 s^{-1} for OP-FRGC-PE, and 174.2 s^{-1} for OP-FRGC-PP, all specimens were crashed into pieces of fragments. Notably, despite the formation of fragments at high strain rates, the presence of fibers in OP-FRGC ensured that most fragments remained interconnected. This phenomenon highlights that the fibers formed a network within the specimens, facilitating effective energy transfer to the matrix and thereby enhancing

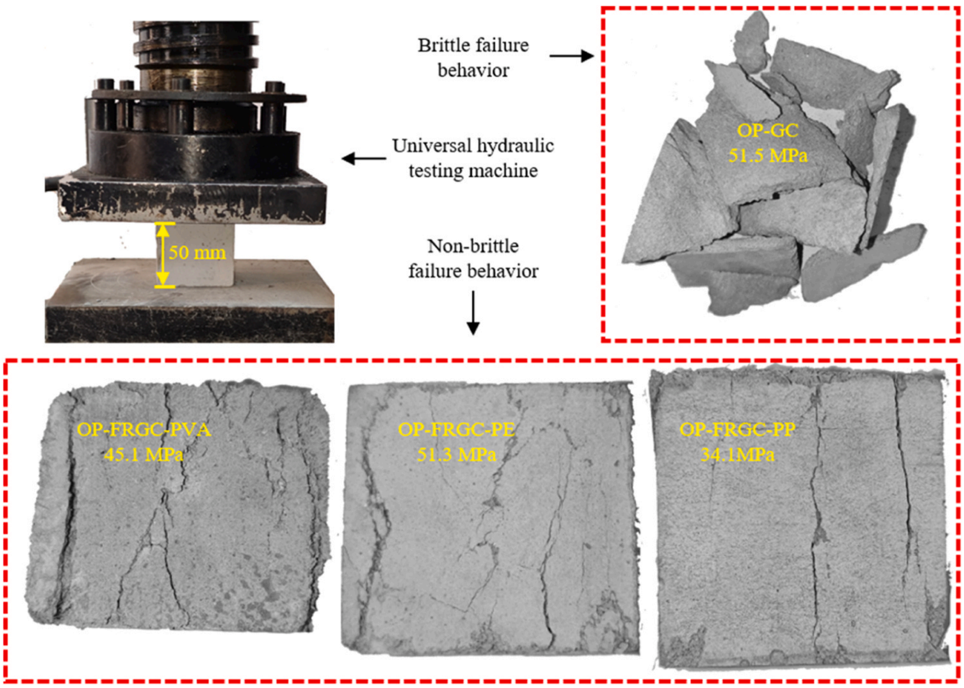

Fig. 6. Quasi-static test of OP-GC and OP-FRGC.

energy absorption capacity.

The occurrence of the observed failure mode can be attributed to the behavior of the material under high strain rate loading, during which cracks between the matrix, interfacial transition zones, and aggregates expand, absorbing the impact energy generated by dynamic loading [44]. Although the fiber bridging effect significantly contributes to crack control under dynamic loading, it is evident that its effectiveness has limitations, especially at very high strain rates. Furthermore, different types of fibers demonstrated varying degrees of bridging efficacy. In particular, PE fiber proved to be the most effective reinforcement due to its higher tensile strength and modulus of elasticity compared to the other two fiber types.

Fig. 8 illustrates the condition of fibers within the specimens after failure under dynamic loading. It can be observed that after dynamic loading, the specimens reinforced with PVA or PE fibers retained connections between many of the matrix fragments through the fibers, despite significant damage to the matrix material. In contrast, the specimens with PP fibers exhibited substantial fiber pull-out and rupture, resulting in relatively weaker connections between the matrix fragments. It should be mentioned that the dispersion of PVA fibers in the matrix was less uniform compared to PE fibers. This uneven distribution can be a factor that led to the lower strength of OP-FRGC-PVA compared to that of OP-FRGC-PE.

Fig. 9 shows the scanning electron microscope (SEM) images of the fibers and fractured matrix. The SEM images revealed that all three OP-FRGC specimens exhibited fiber pull-out and rupture, though the damages varied depending on the fiber type. The PVA fibers were more extensively encased in matrix material compared to the others, which can be attributed to the use of non-oil-coated PVA fibers. The strong chemical bond between PVA fibers and the matrix caused the process of pull-out involving considerable amounts of matrix material.

In contrast, the PP fibers had minimal matrix attached to their surfaces, and there were fewer scratches compared to the other two fiber types, indicating the weakest adhesion between PP fibers and the matrix [14]. As a result, the OP-FRGC-PP specimens cannot effectively prevent early cracking under compressive loading, leading to the lowest strength. On the other hand, the PE fibers exhibited adhesion and scratch similar to those of the PVA fibers. However, owing to their higher elastic modulus and tensile strength [45], fewer PE fibers ruptured during impact under the same strain rate compared to PVA fibers. This behavior demonstrates that the cooperation between PE fibers and the matrix was the most effective among the three types of OP-FRGC specimens.

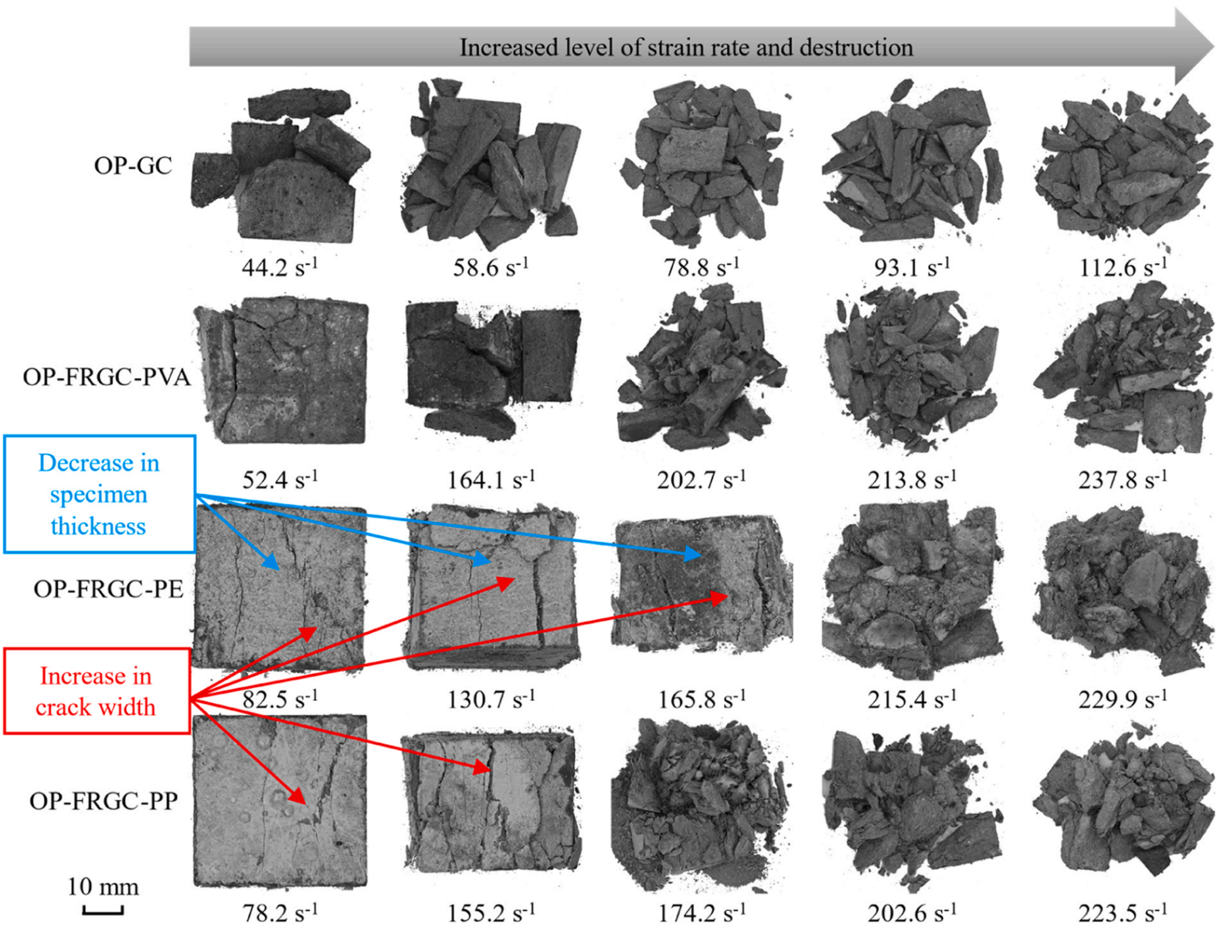

Fig. 7. Failure modes of OP-GC and OP-FRGC under dynamic compression.

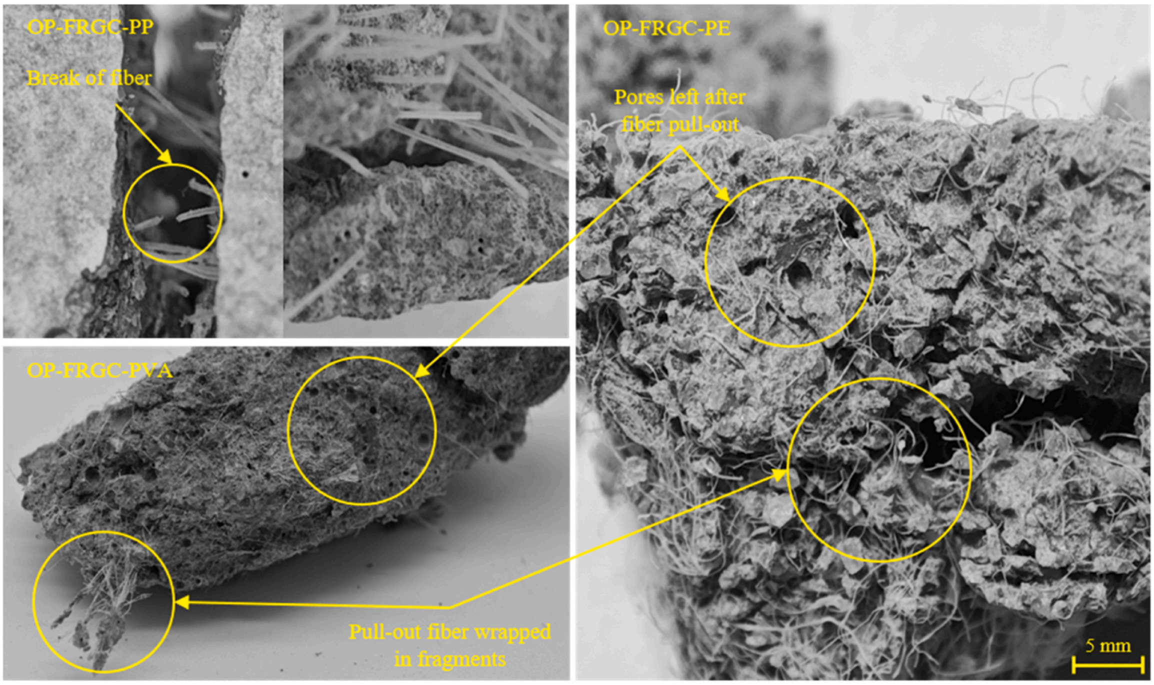

Fig. 8. The state of the fiber within specimen after failure under dynamic compression.

To further demonstrate the role of fibers in OP-FRGC, Fig. 10 presents a schematic diagram of the failure mechanisms of OP-FRGC under dynamic loading. The failure mechanisms can be broadly categorized into three types: (1) Matrix Damage: This occurs when the strong bonding effect and fiber strength, combined with relatively weaker matrix strength, lead to failure around the fiber-matrix interface; (2) Fiber Pull-Out: This results from the insufficient bonding between fibers and matrix, causing the fibers to be pulled out during loading; (3) Fiber Rupture: This occurs due to the strong chemical interaction between the fibers and the matrix, which therefore results in the rupture of the fibers prior to pull-out under relatively high strain rates [46].

In summary, OP-GC, similar to conventional GC, exhibits typical brittle failure characteristics under impact loading. The inclusion of fibers in OP-FRGC introduces a bridging effect, which can effectively limit crack initiation and propagation, thereby reducing the overall damage caused by impact loading. However, the dynamic failure mechanisms vary significantly depending on the bonding characteristics with the matrix and the fiber strength. Among the different fibers studied, PE fibers exhibited the best enhancement effect on OP-GC, providing the most effective improvement in dynamic performance.

3.2.2. *Dynamic stress-strain curve and energy absorption*

Fig. 11 shows the stress-strain curves of OP-GC and OP-FRGC under dynamic compressive loading. All specimens exhibit an initial rise to peak stress, followed by a descending segment until ultimate strain. Notably, fibers typically demonstrate bridging effects after the initial linear rise, absorbing significant energy during the fiber pull-out or rupture [47].

For OP-GC and OP-FRGC-PVA specimens, the descending stage of the curve generally shows a steeper slope, whereas the OP-FRGC-PE specimens exhibit a more gradual slope in the descending region. It is evident that as the strain rate increases, the peak compressive stress also increases, confirming the strain rate dependency of both OP-GC and OP-FRGC. Moreover, the peak strain of OP-FRGC is substantially larger than that of OP-GC. For instance, the peak strain of OP-GC is approximately 0.005, which is half that of OP-FRGC.

The energy absorption of OP-FRGC is calculated by integrating the stress-strain curve of the specimen under dynamic compressive loading. E_c was calculated using the trapezoidal rule. ε_f is the strain at failure. Energy absorption was normalized to unit volume (kJ/m^3), and the equation is given by

$$E_c = \frac{\int_0^{\varepsilon_f} \sigma(\varepsilon) d\varepsilon}{V} \tag{4}$$

where V is the volume of the specimen.

Fig. 12 illustrates the energy absorption of OP-GC and OP-FRGC, and the fitted equations are given by

$$E_c \text{ of OP-GC} = 7.36734\dot{\varepsilon} + 114.92371 \text{ for } 44.2 \leq \dot{\varepsilon} \leq 112.6 \text{ s}^{-1} \tag{5}$$

$$E_c \text{ of OP-FRGC-PVA} = 4.06182\dot{\varepsilon} + 480.08512 \text{ for } 52.4 \leq \dot{\varepsilon} \leq 237.8 \text{ s}^{-1} \tag{6}$$

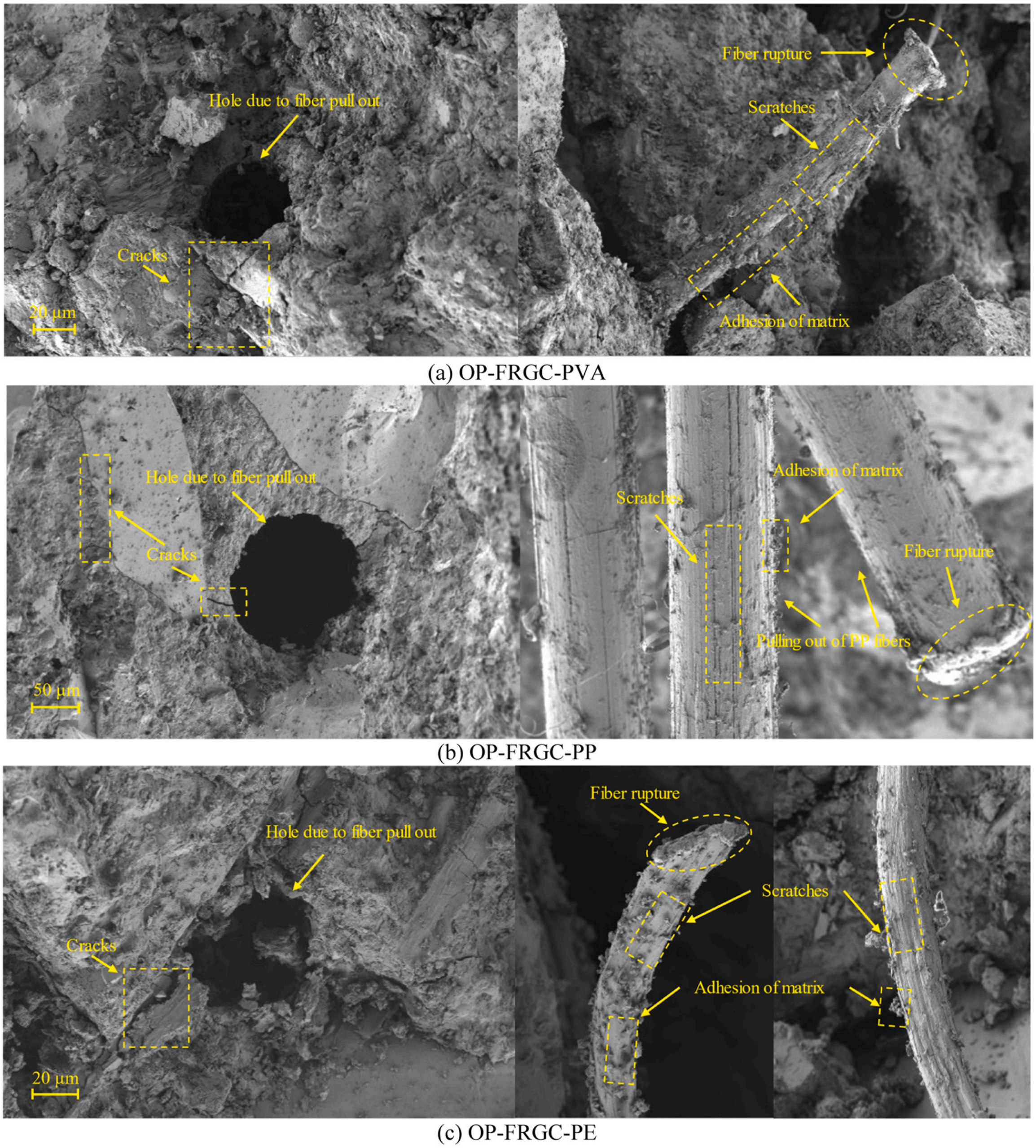

Fig. 9. SEM images of matrix and fibers.

$$E_c \text{ of OP-FRGC-PE} = 6.45101\dot{\varepsilon} + 302.47039 \text{ for } 82.5 \le \dot{\varepsilon} \le 229.9 \text{ s}^{-1} \tag{7}$$

$$E_c \text{ of OP-FRGC-PP} = 6.81231\dot{\varepsilon} + 58.34667 \text{ for } 78.2 \le \dot{\varepsilon} \le 223.5 \text{ s}^{-1} \tag{8}$$

Generally, as the strain rate increases, the energy absorbed under dynamic compression (E_c) also increases linearly. The energy absorption capacity is influenced by both peak strain and compressive strength. At low strain rates, the energy absorption of OP-FRGC is similar to that of OP-GC, as the reduction in compressive strength offsets the increase in peak strain due to fiber inclusion. At higher strain rates, OP-FRGC-PE specimens absorb more energy compared to OP-FRGC-PP and OP-FRGC-PVA. This can be attributed to the high tensile strength and strong bond of PE fibers with the matrix, which enables PE fibers to continue exhibiting excellent bridging effects even under high strain rates, thereby maintaining the energy absorption of OP-FRGC-PE. Therefore, compared to OP-FRGC-PP and OP-FRGC-PVA, OP-FRGC-PE exhibits superior energy absorption capacity. Additionally, the energy absorption data for OP-FRGC-PVA shows greater variability than that of OP-FRGC-PP and OP-FRGC-PE, which is attributable to less effective dispersion of PVA

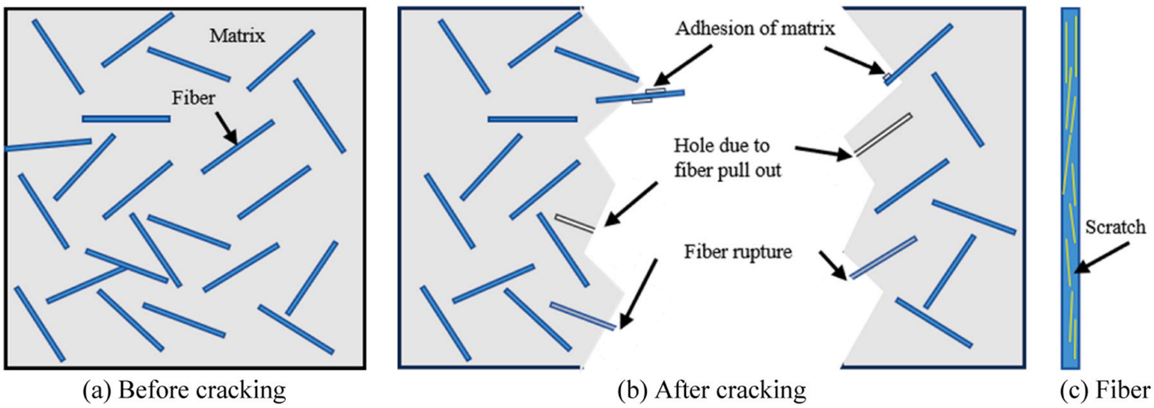

Fig. 10. Schematic drawing of the failure mode of OP-FRGC specimens.

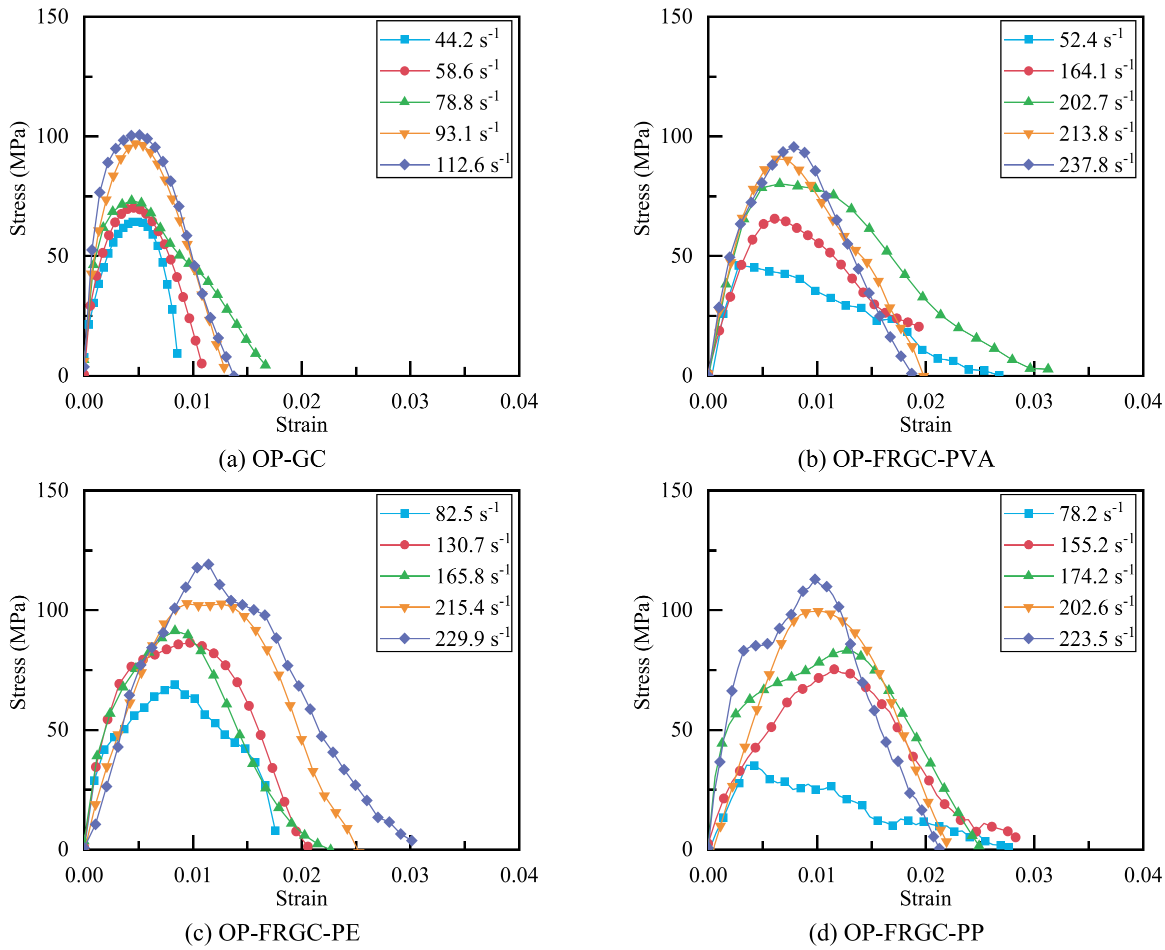

Fig. 11. The strain-stress curves of OP-GC and OP-FRGC.

fibers within the matrix compared to PP and PE fibers.

3.2.3. *Dynamic increase factor*

The compressive strengths of OP-GC and OP-FRGC were measured over a range of strain rates from approximately 40 s^{-1} to 240 s^{-1} . The dynamic strengths are proven to be considerably influenced by high strain rates, as revealed by the SHPB tests. The CDIF is defined as the ratio of the dynamic compressive strength to the quasi-static compressive strength. This factor is frequently used to calculate the

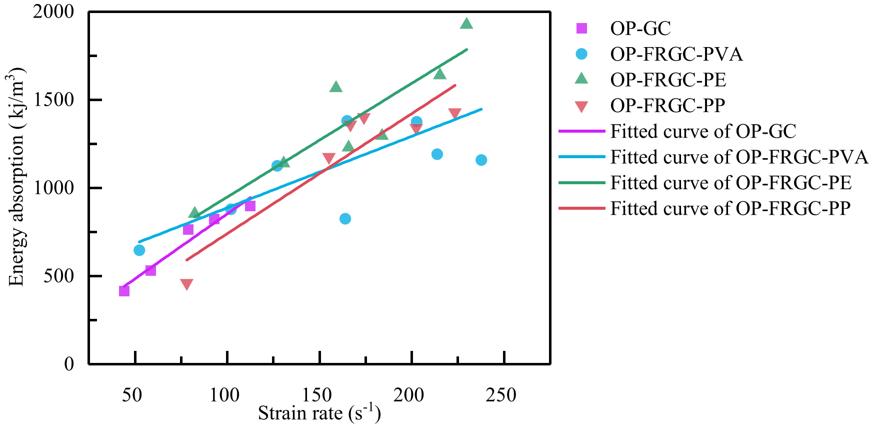

Fig. 12. Energy absorption of OP-GC and OP-FRGC.

enhancement of the material strength under dynamic loading. Based on the test results, the CDIF values of OP-GC and OP-FRGC at various strain rates are shown in Fig. 13. It is observed that the natural logarithm of the strain rate ($\ln\dot{\varepsilon}$) increases practically linearly with the CDIF of OP-GC and OP-FRGC, and the expressions of the fitted curves are given by

$$\text{CDIF of OP-GC} = 0.78773\ln\dot{\varepsilon} - 1.78602 \text{ for } 44.2 \le \dot{\varepsilon} \le 112.6 \text{ s}^{-1} \tag{9}$$

$$\text{CDIF of OP-FRGC-PVA} = 0.62837\ln\dot{\varepsilon} - 1.38688 \text{ for } 52.4 \le \dot{\varepsilon} \le 237.8 \text{ s}^{-1} \tag{10}$$

$$\text{CDIF of OP-FRGC-PE} = 0.731\ln\dot{\varepsilon} - 1.8827 \text{ for } 82.5 \le \dot{\varepsilon} \le 229.9 \text{ s}^{-1} \tag{11}$$

$$\text{CDIF of OP-FRGC-PP} = 2.0105\ln\dot{\varepsilon} - 7.75866 \text{ for } 78.2 \le \dot{\varepsilon} \le 223.5 \text{ s}^{-1} \tag{12}$$

It is also observed that the fitted curves for OP-GC, OP-FRGC-PVA, and OP-FRGC-PE have similar slopes of 0.78773, 0.62837, and 0.731, respectively. In contrast, the fitted curve for OP-FRGC-PP has a significantly higher slope of 2.0105, indicating a greater sensitivity to strain rates. This difference can be explained as follows: under quasi-static loading or at relatively low strain rates, the weak bonding between PP fibers and the matrix results in a limited bridging effect, leading to relatively low strength. However, at higher strain rates, the bridging effect of PP fibers becomes more pronounced, helping to maintain the integrity of the specimen as a whole. In addition, microvoids within the specimen are compressed under high strain rates, which results in substantially higher dynamic strength and consequently a larger CDIF.

The test results from this investigation are also compared with those from previously published studies [20,23,48,49], as shown in Fig. 13. The fitted CDIF curve for OP-GC closely aligns with the *fib* Model Code [48], while the fitted curves for OP-FRGC-PVA and OP-FRGC-PE are comparable to those reported by Khan et al. [20]. However, most data points for OP-FRGC-PVA and OP-FRGC-PE fall below the *fib* Model Code [48] recommendations, suggesting that the current model is suitable for OP-GC but tends to overestimate the dynamic compressive strength of OP-FRGC-PVA and OP-FRGC-PE.

In the study by Zhang et al. [23], GPC-SP and GPC-PP denote specimens incorporating 0.5 % steel fibers with 0.5 % PP fibers and 1 % PP fibers, respectively. The fitted CDIF curves for OP-FRGC-PP were found to be more similar to GPC-SP than to GPC-PP. The

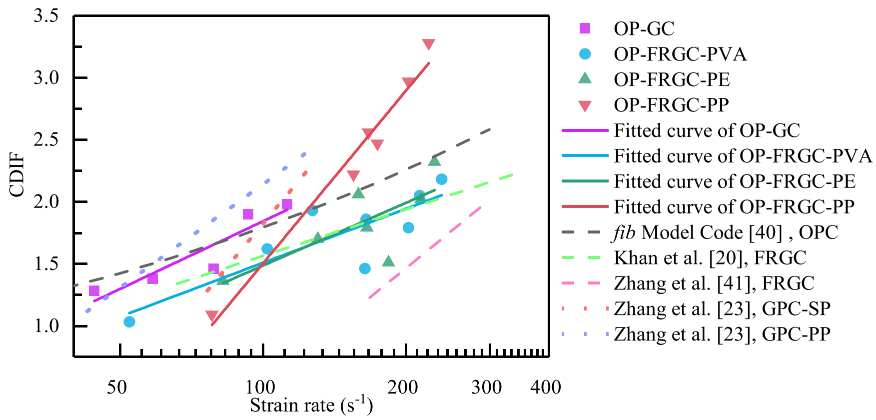

Fig. 13. CDIFs of OP-FRGC and OP-GC and comparison with previous studies.

observed differences in CDIF among these studies may be attributed to variations in specimen size and shape, matrix composition, and fiber type, size, and content. Despite these differences, OP-FRGC exhibits strain rate sensitivities comparable to those of conventional alkaline solution-activated FRGC. Table 5 summarizes all the test results for OP-GC and OP-FRGC under dynamic compressive loading.

4. Comprehensive assessment of OP-FRGC considering sustainability

It is important to note that dynamic mechanical properties should not be the sole basis for comparing different OP-FRGC. The assessment should also consider the sustainability and cost of the materials. Sustainability is assessed using a standardized approach known as life cycle assessment (LCA), which involves embodied carbon and embodied energy. Embodied carbon is the total greenhouse gas emissions associated with the production, transportation, and construction of materials. In contrast, embodied energy is the total energy consumed over the entire lifecycle of a material, including extraction, manufacturing, transportation, and installation. Both indicators are widely regarded as key metrics for evaluating the environmental impact of construction materials, especially considering the construction industry's significant share in global carbon emissions. By focusing on embodied carbon, the potential of OP-FRGC to reduce carbon footprints compared to conventional cement-based materials is highlighted. Additionally, evaluating embodied energy enables the quantification of energy savings achieved through the use of OP-FRGC, which incorporates industrial by-products, e.g., FA and GGBS, as substitutes for energy-intensive OPC. For a comprehensive evaluation of OP-FRGC, six indices including quasi-static compressive strength, dynamic compressive strength, energy absorption, embodied carbon, embodied energy, and cost were selected as key indicators. Table 6 presents the costs and sustainability indicators of raw materials. The data were derived from previous research [50–54].

Before evaluating the sustainability and material costs of OP-FRGC, it is essential to assess these aspects for the one-part geopolymer matrix itself. The calculation process is detailed in Table 7. Owing to the widespread availability and utilization of GGBS and FA, the embodied carbon of one-part geopolymer is relatively low, at only 206.7 $kgCO_2$·eq/t, while its embodied energy is 1075 MJ/t. Notably, these values are approximately one-fifth of those associated with OPC. In addition, the cost of OPG is 241.25 CNY/t, which is approximately 63 % of that of OPC. As a result, one-part geopolymer can replace OPC in fiber-reinforced composites, thereby significantly lowering carbon emissions and cost.

Fig. 14 presents the sustainability and material costs of OP-FRGC. The embodied carbon values for OP-FRGC-PE, OP-FRGC-PVA, and OP-FRGC-PP are similar, each being approximately 650 $kgCO_2$·eq/m^3. Among these composites, OP-FRGC-PP exhibits the lowest embodied energy, at 2483 MJ/m^3, while OP-FRGC-PVA shows the highest, at 3093 MJ/m^3. The differences in material costs among the composites with different fiber types are particularly significant. Specifically, the cost of OP-FRGC-PP is the lowest, at 1172 CNY/m^3, whereas OP-FRGC-PE has the highest cost, reaching 2708 CNY/m^3.

According to the Technique for Order Preference by Similarity to Ideal Solution (TOPSIS) [55], the indicators are classified as minimization indicators (embodied carbon, embodied energy, and cost) and maximization indicators (quasi-static and dynamic compressive strength, energy absorption). Minimization indicators naturally benefit from lower values, implying that "less is better." Maximization indicators inherently benefit from higher values, indicating that "more is better." Such variables are classified as maximizing indicators because the objective is to maximize them for improved performance. Transforming minimization indicators into their maximizing counterparts ensures that all variables are assessed on a uniform "higher-is-better" scale. This uniform approach simplifies the comparison of diverse metrics. Before the assessment, all indicators must be standardized, with minimization indicators must be transformed into their maximizing counterparts. After normalization, the results are presented in Fig. 15. Despite possessing significant advantages in mechanical performance and embodied carbon, the high cost of OP-FRGC-PE restricts its potential for widespread application. In contrast, OP-FRGC-PVA does not offer notable advantages concerning cost, sustainability, or mechanical performance. In comparison, the indicators for OP-FRGC-PP are relatively well-balanced, making it a more favorable option overall.

5. Conclusion

The dynamic compressive properties of OP-FRGC containing various fiber types were examined in this study. A comprehensive assessment of OP-FRGC with various fibers types was also conducted. Conclusions are drawn as follows:

1. The dynamic compressive mechanical properties of OP-FRGC were similar to those of conventional alkali solution-activated FRGC. In particular, the CDIF of OP-FRGC with various fiber types exhibited a trend comparable to that of conventional FRGC.
2. The damage severity increased with strain rate during dynamic compression, leading to broader cracks and smaller pieces. OP-GC exhibited brittle damage features at strain rates below 50 s^{-1}, whereas OP-FRGC, particularly OP-FRGC-PE, typically fractured into pieces at strain rates exceeding 150 s^{-1}.
3. OP-FRGC demonstrated strain rate sensitivity under dynamic compression, with the CDIF increasing approximately linearly with the natural logarithm of the strain rate. The types of fibers influenced the CDIF of OP-FRGC. In particular, OP-FRGC-PP, OP-FRGC-PVA, and OP-FRGC-PE achieved the CDIF of 3.28, 2.18, and 2.32 at the strain rate of 223.5 s^{-1}, 237.8 s^{-1}, and 229.9 s^{-1}, respectively.
4. Among PE, PP, and PVA fibers, PE fibers provided the most substantial improvement in failure mode and energy absorption, while OP-FRGC-PP demonstrated the highest strain rate sensitivity.
5. Compared to OPC, one-part geopolymer offers significant economic and sustainability benefits. The material cost of one-part geopolymer is about 37 % less than that of OPC, and the embodied carbon and energy of one-part geopolymer are approximately 20 % of those associated with OPC.

Table 5
Tests results of OP-FRGC and OP-GC specimens.

Specimen	Strain rate (s^{-1})	Dynamic compressive strength (MPa)	CDIF	Energy absorption (kJ/m^3)
OP-GC−1	44.2	65.9	1.28	412.38
OP-GC−2	58.6	71.1	1.38	531.43
OP-GC−3	78.8	75.2	1.46	763.65
OP-GC−4	93.1	97.9	1.90	823.64
OP-GC−5	112.6	102.0	1.98	896.89
OP-FRGC-PVA−1	52.4	46.5	1.03	645.34
OP-FRGC-PVA−2	102.1	73.1	1.62	877.64
OP-FRGC-PVA−3	127.2	87.0	1.93	1125.78
OP-FRGC-PVA−4	164.1	65.8	1.46	825.04
OP-FRGC-PVA−5	165.1	83.9	1.86	1380.4
OP-FRGC-PVA−6	202.7	80.7	1.79	1374.19
OP-FRGC-PVA−7	213.8	92.5	2.05	1191.56
OP-FRGC-PVA−8	237.8	98.3	2.18	1158.55
OP-FRGC-PE−1	82.5	69.8	1.36	852.2
OP-FRGC-PE−2	130.7	87.2	1.70	1139.08
OP-FRGC-PE−3	159.0	105.7	2.06	1566.63
OP-FRGC-PE−4	165.8	91.8	1.79	1229.01
OP-FRGC-PE−5	183.9	77.5	1.51	1295.15
OP-FRGC-PE−6	215.4	103.6	2.02	1639.39
OP-FRGC-PE−7	229.9	119.0	2.32	1925.45
OP-FRGC-PP−1	78.2	37.2	1.09	460.17
OP-FRGC-PP−2	155.2	75.7	2.22	1174.96
OP-FRGC-PP−3	166.9	87.3	2.56	1360.13
OP-FRGC-PP−4	174.2	84.2	2.47	1400.79
OP-FRGC-PP−5	202.6	101.3	2.97	1340.94
OP-FRGC-PP−6	223.5	111.8	3.28	1429.49

Table 6
Costs and sustainability indicators of raw materials.

Type	Embodied carbon ($kgCO_2$·eq/t)	Embodied energy (MJ/t)	Cost (CNY/t)
Na_2SiO_3	1860	9400	860
Quartz sand	580	850	280
HRWR	1880	11,470	60,000
Water	0.8	10	7
PP	3100	77,240	44,415
PVA	3400	101,000	60,000
PE	2000	94,500	200,000
FA	4	100	155
GGBS	42	200	190
OPC	912	5500	385

Table 7
Sustainability and costs of one-part geopolymer.

Raw Materials	Mix proportions (kg/t)	Embodied carbon ($kgCO_2$·eq/t)	Embodied energy (MJ/t)	Cost (CNY/t)
FA	450	4	100	155
GGBS	450	42	200	190
Na_2SiO_3	100	1860	9400	860
One-part geopolymer	-	206.7	1075	241.25

6. Without considering cost, OP-FRGC-PE exhibited optimal static and dynamic mechanical properties as well as sustainability performance. However, when cost is considered, OP-FRGC-PP demonstrated a more balanced performance across all evaluated aspects.

It should be noted that this study focused on three types of fibers (PVA, PE, and PP) at a fixed volume fraction of 1 %. Varying the fiber content or using hybrid fiber types may lead to different outcomes, which warrant further investigation. In addition, this study primarily examines the dynamic compressive performance of OP-FRGC, while its dynamic tensile performance deserves further exploration.

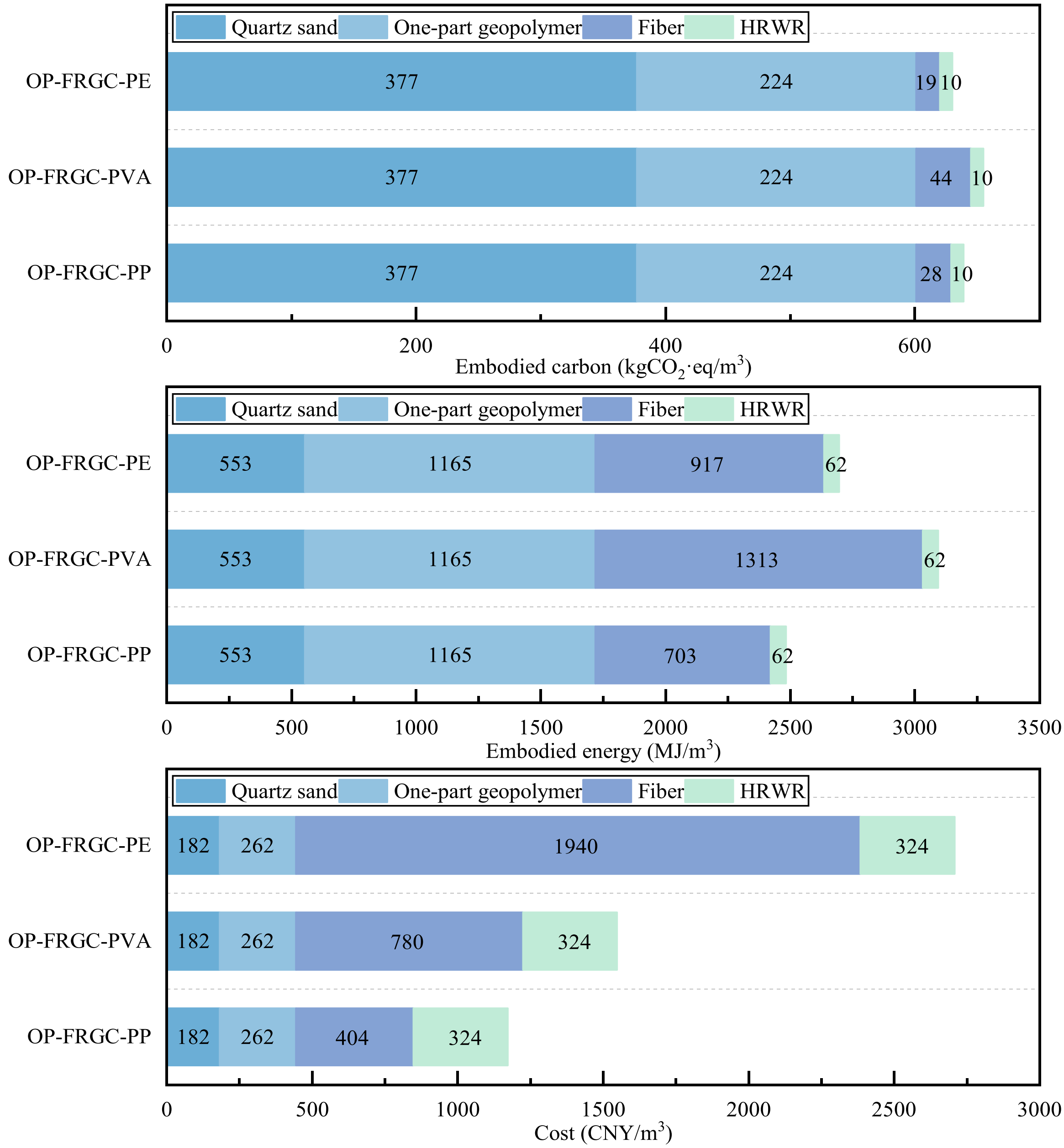

Fig. 14. Comparison of sustainability and costs of OP-FRGC.

CRediT authorship contribution statement

Hanyuan Shi: Investigation, Formal analysis, Data curation, Writing – original draft. **Qian Zang:** Data curation, Investigation. **Yingfan Wang:** Data curation, Investigation. **Haimin Qian:** Funding acquisition, Investigation. **Zhouhong Zong:** Supervision, Resources. **Jingming Cai:** Funding acquisition, Resources, Conceptualization. **Mei Li:** Investigation. **Yuanzheng Lin:** Funding acquisition, Supervision, Resources, Writing – review & editing.

Declaration of Competing Interest

The authors declare that they have no known competing financial interests or personal relationships that could have appeared to influence the work reported in this paper.

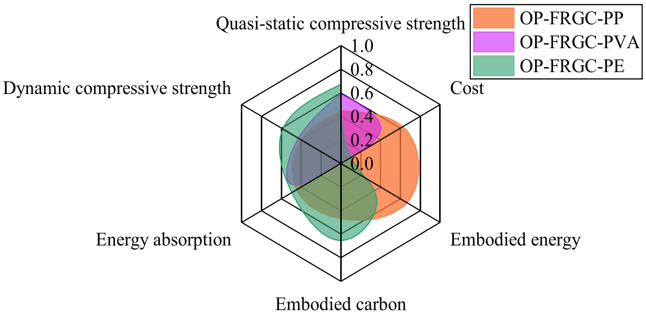

Fig. 15. Comprehensive assessment of OP-FRGC with different fibers.

Acknowledgments

This work was financially supported by the Zhejiang Engineering Research Center of Intelligent Urban Infrastructure (No. IUI2023-YB-02), the Opening Project of State Key Laboratory of Explosion Science and Technology (Beijing Institute of Technology) (No. KFJJ23-13M), and the National Natural Science Foundation of China (No. 52308535).

Data availability

Data will be made available on request.

References

[1] D.L.Y. Kong, J.G. Sanjayan, Damage behavior of geopolymer composites exposed to elevated temperatures, Cem. Concr. Compos. 30 (10) (2008) 986–991.
[2] A. Palomo, M.W. Grutzeck, M.T. Blanco, Alkali-activated fly ashes: a cement for the future, Cem. Concr. Res. 29 (8) (1999) 1323–1329.
[3] T. Bakharev, Geopolymeric materials prepared using Class F fly ash and elevated temperature curing, Cem. Concr. Res. 35 (6) (2005) 1224–1232.
[4] E. Papa, V. Medri, S. Amari, J. Manaud, P. Benito, A. Vaccari, E. Landi, Zeolite-geopolymer composite materials: production and characterization, J. Clean. Prod. 171 (2018) 76–84.
[5] J.N.Y. Djobo, D. Stephan, Control of the setting reaction and strength development of slag-blended volcanic ash-based phosphate geopolymer with the addition of boric acid, J. Aust. Ceram. Soc. 57 (4) (2021) 1145–1154.
[6] A. Hajimohammadi, J.L. Provis, J.S.J. van Deventer, One-part geopolymer mixes from geothermal silica and sodium aluminate, Ind. Eng. Chem. Res. 47 (23) (2008) 9396–9405.
[7] C. Ma, B. Zhao, S. Guo, G. Long, Y. Xie, Properties and characterization of green one-part geopolymer activated by composite activators, J. Clean. Prod. 220 (2019) 188–199.
[8] N. Ye, J. Yang, S. Liang, Y. Hu, J. Hu, B. Xiao, Q. Huang, Synthesis and strength optimization of one-part geopolymer based on red mud, Constr. Build. Mater. 111 (2016) 317–325.
[9] B. Nematollahi, J. Sanjayan, F.U.A. Shaikh, Synthesis of heat and ambient cured one-part geopolymer mixes with different grades of sodium silicate, Ceram. Int. 41 (4) (2015) 5696–5704.
[10] P.K. Sarker, R. Haque, K.V. Ramgolam, Fracture behaviour of heat cured fly ash based geopolymer concrete, Mater. Des. 44 (2013) 580–586.
[11] R.J. Thomas, S. Peethamparan, Alkali-activated concrete: engineering properties and stress–strain behavior, Constr. Build. Mater. 93 (2015) 49–56.
[12] N. Ranjbar, M. Zhang, Fiber-reinforced geopolymer composites: a review, Cem. Concr. Compos. 107 (2020) 103498.
[13] J. Cai, J. Pan, J. Han, Y. Lin, Z. Sheng, Impact behaviours of engineered geopolymer composite exposed to elevated temperatures, Constr. Build. Mater. 312 (2021) 125421.
[14] J. Han, J. Cai, Y. Lin, Y. Sun, J. Pan, Impact resistance of engineered geopolymer composite (EGC) in cold temperatures, Constr. Build. Mater. 343 (2022) 128150.
[15] J. Cai, J. Pan, J. Han, Y. Lin, Z. Sheng, Low-energy impact behavior of ambient cured engineered geopolymer composites, Ceram. Int. 48 (7) (2022) 9378–9389.
[16] Y. Lin, Y. Wang, S. Wan, C. Yang, Z. Zong, H. Qian, X. Xu, M. Elchalakani, J. Cai, Experimental studies on behavior of one-part geopolymer composite slabs subjected to blast loading, Structures 66 (2024) 106825.
[17] H. Fan, H. Yu, H. Ma, Dynamic increase factor(DIF) of concrete with SHPB tests: review and systematic analysis, J. Build. Eng. 79 (2023) 107666.
[18] X. Luo, J.-y Xu, E.-l Bai, W. Li, Research on the dynamic compressive test of highly fluidized geopolymer concrete, Constr. Build. Mater. 48 (2013) 166–172.
[19] S.-H. Xiao, S.-J. Liao, G.-Q. Zhong, Y.-C. Guo, J.-X. Lin, Z.-H. Xie, Y. Song, Dynamic properties of PVA short fiber reinforced low-calcium fly ash - slag geopolymer under an SHPB impact load, J. Build. Eng. 44 (2021) 103220.
[20] M.Z.N. Khan, Y. Hao, H. Hao, Fu.A. Shaikh, Mechanical properties and behaviour of high-strength plain and hybrid-fiber reinforced geopolymer composites under dynamic splitting tension, Cem. Concr. Compos. 104 (2019) 103343.
[21] M.Z.N. Khan, Y. Hao, H. Hao, F.U.A. Shaikh, Experimental evaluation of quasi-static and dynamic compressive properties of ambient-cured high-strength plain and fiber reinforced geopolymer composites, Constr. Build. Mater. 166 (2018) 482–499.
[22] H. Zhong, M. Zhang, Effect of recycled polymer fibre on dynamic compressive behaviour of engineered geopolymer composites, Ceram. Int. 48 (16) (2022) 23713–23730.
[23] H. Zhang, T.C. Jia, P.K. Sarker, W. Chen, Q. Wang, Z. Li, B. He, Z. Jiang, Effect of fibre addition on the static and dynamic compressive properties of ambient-cured geopolymer concrete, J. Build. Eng. 58 (2022) 104991.
[24] L.-Y. Xu, J.-C. Lao, L.-P. Qian, M. Khan, T.-Y. Xie, B.-T. Huang, Low-carbon high-strength engineered geopolymer composites (HS-EGC) with full-volume fly ash precursor: role of silica modulus, J. CO2 Util. 88 (2024) 102948.
[25] J.-C. Lao, B.-T. Huang, Y. Fang, L.-Y. Xu, J.-G. Dai, S.P. Shah, Strain-hardening alkali-activated fly ash/slag composites with ultra-high compressive strength and ultra-high tensile ductility, Cem. Concr. Res. 165 (2023) 107075.
[26] J.-C. Lao, B.-T. Huang, L.-Y. Xu, M. Khan, Y. Fang, J.-G. Dai, Seawater sea-sand engineered geopolymer composites (EGC) with high strength and high ductility, Cem. Concr. Compos. 138 (2023) 104998.
[27] J.-C. Lao, R.-Y. Ma, L.-Y. Xu, Y. Li, Y.-N. Shen, J. Yao, Y.-S. Wang, T.-Y. Xie, B.-T. Huang, Fly ash-dominated high-strength engineered/strain-hardening geopolymer composites (HS-EGC/SHGC): influence of alkalinity and environmental assessment, J. Clean. Prod. 447 (2024) 141182.

[28] Y. Lin, C. Yang, H. Shi, Y. Wang, Z. Zong, H. Qian, S. Hou, S. Li, T. Chen, J. Cai, Dynamic mechanical properties of one-part ultra-high performance geopolymer concrete, J. Build. Eng. 95 (2024) 110173.
[29] Y. Zhou, Z. Hu, X. Sui, H. Shi, Y. Lin, J. Pan, N. Ukrainczyk, J. Cai, Low-velocity impact behavior of one-part engineered geopolymer composite under extreme temperatures, Compos. Part A Appl. Sci. Manuf. 191 (2025) 108739.
[30] Q. Zhao, C. Ma, B. Huang, X. Lu, Development of alkali activated cementitious material from sewage sludge ash: two-part and one-part geopolymer, J. Clean. Prod. 384 (2023) 135547.
[31] I.P. Segura, T. Luukkonen, J. Yliniemi, H. Sreenivasan, A.J. Damø, L.S. Jensen, M. Canut, A.M. Kantola, V.-V. Telkki, P.A. Jensen, Comparison of one-part and two-part alkali-activated metakaolin and blast furnace slag, J. Sustain. Metall. 8 (4) (2022) 1816–1830.
[32] Y. Lin, Y. Yuan, S. Wan, B. Ding, C. Yang, Z. Zong, X. Gu, J. Cai, Flexural behaviour of reinforced one-part geopolymer concrete beams, J. Build. Eng. 96 (2024) 110435.
[33] Y. Yuan, B. Ding, H. Shi, Y. Wang, Y. Lin, M. Elchalakani, J. Cai, Flexural behaviour of one-part fibre-reinforced geopolymer beams, J. Build. Eng. 91 (2024) 109538.
[34] T. Luukkonen, Z. Abdollahnejad, J. Yliniemi, P. Kinnunen, M. Illikainen, One-part alkali-activated materials: a review, Cem. Concr. Res. 103 (2018) 21–34.
[35] J. Cai, J. Tan, X. Li, Thermoelectric behaviors of fly ash and metakaolin based geopolymer, Constr. Build. Mater. 237 (2020) 117757.
[36] L. Zhang, Y. Wang, B. Ding, J. Gu, J. Cai, Study on the mechanical and thermal properties of one-part geopolymer composite for high performance in energy piles, Case Stud. Constr. Mater. 19 (2023) e02230.
[37] J. Tan, J. Cai, X. Li, J. Pan, J. Li, Development of eco-friendly geopolymers with ground mixed recycled aggregates and slag, J. Clean. Prod. 256 (2020) 120369.
[38] M. Li, H. Hao, Y. Shi, Y. Hao, Specimen shape and size effects on the concrete compressive strength under static and dynamic tests, Constr. Build. Mater. 161 (2018) 84–93.
[39] W. Chen, B. Song, Split Hopkinson (Kolsky) Bar: Design, Testing and Applications, Springer, New York, NY, 2011.
[40] Y. Hao, H. Hao, Dynamic compressive behaviour of spiral steel fibre reinforced concrete in split hopkinson pressure bar tests, Constr. Build. Mater. 48 (2013) 521–532.
[41] Z. Yin, W. Chen, H. Hao, J. Chang, G. Zhao, Z. Chen, K. Peng, Dynamic compressive test of gas-containing coal using a modified split hopkinson pressure bar system, Rock. Mech. Rock. Eng. 53 (2) (2020) 815–829.
[42] Z. Huang, W. Chen, H. Hao, R. Aurelio, Z. Li, M. Pham Thong, Test of dynamic mechanical properties of ambient-cured geopolymer concrete using split hopkinson pressure bar, J. Mater. Civ. Eng. 34 (2) (2022) 04021440.
[43] H. Li, X. Li, J. Fu, N. Zhu, D. Chen, Y. Wang, S. Ding, Experimental study on compressive behavior and failure characteristics of imitation steel fiber concrete under uniaxial load, Constr. Build. Mater. 399 (2023) 132599.
[44] S. Wang, H.T.N. Le, L.H. Poh, S.T. Quek, M.-H. Zhang, Effect of high strain rate on compressive behavior of strain-hardening cement composite in comparison to that of ordinary fiber-reinforced concrete, Constr. Build. Mater. 136 (2017) 31–43.
[45] J. Cai, J. Pan, Y. Lin, J. Han, B. Ding, N. Ukrainczyk, Effect of temperature on the low-velocity impact behaviors of engineered cementitious composite, J. Mater. Civ. Eng. 35 (7) (2023) 04023167.
[46] J.-X. Lin, Y. Song, Z.-H. Xie, Y.-C. Guo, B. Yuan, J.-J. Zeng, X. Wei, Static and dynamic mechanical behavior of engineered cementitious composites with PP and PVA fibers, J. Build. Eng. 29 (2020) 101097.
[47] Q. Yu, W. Zhuang, C. Shi, Research progress on the dynamic compressive properties of ultra-high performance concrete under high strain rates, Cem. Concr. Compos. 124 (2021) 104258.
[48] fib, fib Model Code for Concrete Structures 2010, Ernst & Sohn, Berlin, Germany, 2013.
[49] D. Zhang, H. Tu, Y. Li, Y. Weng, Effect of fiber content and fiber length on the dynamic compressive properties of strain-hardening ultra-high performance concrete, Constr. Build. Mater. 328 (2022) 127024.
[50] W.-J. Long, Z. Wu, K.H. Khayat, J. Wei, B. Dong, F. Xing, J. Zhang, Design, dynamic performance and ecological efficiency of fiber-reinforced mortars with different binder systems: ordinary portland cement, limestone calcined clay cement and alkali-activated slag, J. Clean. Prod. 337 (2022) 130478.
[51] H. Ye, B. Zhu, P. Ping, Y. Lin, J. Cai, J. Pan, Mechanical performance, impact behavior and environmental assessment of coal furnace slag based low-carbon ultra-high performance engineered cementitious composites (UHP-ECC), J. Clean. Prod. 450 (2024) 141921.
[52] H. Ye, B. Zhu, J. Pan, X. Chen, G. Qu, Solid waste-based low-carbon autoclaved aerated concrete: relationship between engineering properties and microstructure, J. Build. Eng. 91 (2024) 109691.
[53] H. Zhu, D. Zhang, T. Wang, H. Wu, V.C. Li, Mechanical and self-healing behavior of low carbon engineered cementitious composites reinforced with PP-fibers, Constr. Build. Mater. 259 (2020) 119805.
[54] M.L. Marceau, M.A. Nisbet, M.G. VanGeem. Life cycle inventory of portland cement manufacture, Portland Cement Association, Skokie, IL, USA, 2006.
[55] S. Chakraborty, TOPSIS and modified TOPSIS: a comparative analysis, Decis. Anal. J. 2 (2022) 100021.